Available online at www.ujpronline.com
Universal Journal of Pharmaceutical Research
An International Peer Reviewed Journal
ISSN: 2831-5235 (Print); 2456-8058 (Electronic)

RESEARCH ARTICLE

COMPUTATIONAL DRUG REPROPOSING TO IDENTIFY SARS-COV-2 MPRO INHIBITORS: MOLECULAR DOCKING, ADMET ANALYSIS, AND *IN-SILICO/IN-VITRO* TOXICITY STUDY

Mohammed Farrag El-Behairy[1], Marwa AA Fayed[2*], Rasha M. Ahmed[3], Inas A. Abdallah[4]
[1]*Department of Organic and Medicinal Chemistry, Faculty of Pharmacy, University of Sadat City, Sadat City, Egypt.*
[2]*Department of Pharmacognosy, Faculty of Pharmacy, University of Sadat City, Sadat City, Egypt.*
[3]*Department of Pharmaceutical Chemistry, Faculty of Pharmacy, Misr International University, Cairo, Egypt.*
[4]*Department of Analytical Chemistry, Faculty of Pharmacy, University of Sadat City, Sadat City, Egypt.*

Article Info:

Article History:
Received: 5 August 2023
Reviewed: 9 September 2023
Accepted: 20 October 2023
Published: 15 November 2023

Cite this article:
El-Behairy MF, Fayed MAA, Ahmed RM, Abdallah IA. Computational drug reproposing to Identify SARS-CoV-2 Mpro Inhibitors: Molecular Docking, ADMET analysis, and *in-silico/in-vitro* toxicity study. Universal Journal of Pharmaceutical Research 2022; 7(5):23-31.
https://doi.org/10.22270/ujpr.v7i5.837

***Address for Correspondence:**
Dr. Marwa AA Fayed, Department of Pharmacognosy, Faculty of Pharmacy, University of Sadat City, Sadat City, Egypt.
E-mail: *marwa.fayed@fop.usc.edu.eg*

Abstract

Aim and Objective: After the COVID-19 outbreak, drug repurposing has emerged as an effective and fast approach for combating the SARS-CoV-2 crisis. in this work, computational drug repurposing has been utilized to identify new SARS-CoV-2Mpro inhibitors.
Methods: Comparative molecular docking studies were used to evaluate the activity of the commercially available oral antiviral drug simeprevir and its degradation products (compounds 1–5) against the main protease (Mpro) of SARS-CoV-2 (PDB (Protein Data Bank) ID: 6lu7; resolution: 2.16 Å). Moreover, the ADMET and *in-silico* toxicity properties of the acidic (compounds 1–3) and oxidative (compounds 4 and 5) degradation products of simeprevir were predicted.
Results: Docking studies revealed good binding affinities for compounds (1–5) against Mpro of SARS-CoV-2, with binding free energies ranging from −6.23 to−7.65 kcal/mol. The acidic degradant 2 exhibited the best affinity and was superior to simeprevir and a natural ligand. All compounds were expected to be safe to the CNS.
Conclusion: Compounds 1, 4, and 5 were expected to possess good human intestinal absorption, whereas compounds 2 and 3 appeared to have moderate intestinal absorption.
Keywords: ADMET; Computational chemistry; COVID-19; fragment-based drug discovery; Simeprevir; Structure–activity relationships.

INTRODUCTION

The severe acute respiratory syndrome is a result of (SARS-CoV-2), which belongs to the subfamily *Coronavirinae*, family *Coronaviridae*, and affects the respiratory system, causing a severe acute respiratory syndrome. In March of 2020, the WHO proclaimed COVID-19 a worldwide pandemic. It expanded from Wuhan, a crowded city in China, across China, and was then transferred to most other countries of the world[1]. As a specific vaccine for COVID-19, either for prophylaxis or treatment to prevent mortality, is lacking, the search for a quick and effective therapeutic protocol for this disease became a prominent challenge worldwide.

In fact, *de novo* drug discovery has long been recognized as a long and costly process, especially in pandemic circumstances, with a total average cost of $2 to $3 billion and taking at least 13-15 years to reach market availability[2]. During the 1990s, high-throughput screening was introduced as a tool to facilitate and hasten drug discovery[3] however, chemical libraries still need to be prepared through a highly laborious synthetic approach[4]. A dramatic change occurred after the evolution of protein crystallography and NMR that gave access to well-characterized protein-ligand complexes, which have guided drug-lead optimization in terms of selectivity and potency[5]. Simultaneously, computational methods have been utilized for the calculation of molecular interactions, identification of protein-ligand complexes, and screening of chemical libraries against a molecular target[6].

Based on the successful drug repurposing stories in the drug market[7], drug repurposing (also called drug repositioning or drug profiling) has been introduced as a useful tool to decrease costs and save time in drug discovery. This approach depends on finding a new indication for an already existing FDA-approved drug[8].

In addition to the drug indication, which is available, a full descriptive drug profile, including pharmaco-kinetics, pharmacodynamics, and toxicological studies, is also necessary; all of this pre-existing drug information saves time and reduces the research efforts in reaching the new drug indication[9].

After the COVID-19 outbreak in December 2019, drug repurposing was chosen as an effective and fast way to manage the SARS-CoV-2 crisis compared with the long cycle of *de novo* drug discovery[10]. In addition to drug repurposing, computational methods were of great interest to many researchers, which led to the dawn of "*in-silico* repurposing," especially that of pre-existing broad-spectrum antivirals, as this will help shorten the investigation time for any hit compound termed "the drug that will hit the molecular target" to be tested directly in Phase 2 clinical trials. Therefore, by adopting this approach, a new treatment may emerge rapidly and help end this worldwide crisis[11].

Simeprevir is among the pre-existing broad-spectrum antivirals. It is a direct-acting antiviral with a macrocyclic structure (Figure 1) that was originally used for the treatment of genotype I hepatitis C (HCV)[12]. It is a specific and potent inhibitor of the NS3/4A protease, which is an enzyme that is essential for the life cycle of HCV because viral replication is disrupted by the inhibition of the NS3/4A protease[12]. Infact, the mechanism of entry of corona viruses into cells occurs via the action of cellular proteases (i.e., human airway trypsin-like protease, cathepsins, and transmembrane protease serine 2 (TMPRSS2)), which split the spike protein of the virus and cause further penetration alterations[13]. It has been reported that proteases can be inhibited in SARS-CoV-2 by compounds targeting other viral proteases[14]. Moreover, it was reported that simeprevir may be used for the treatment of other viral infections, such as HIV/AIDS[15]. Therefore, testing simeprevir against the SARS-CoV-2 protease may be helpful for the treatment of COVID-19.

The principal feature of fragment-based drug discovery (FBDD) is the screening of a small library of low-molecular-weight compounds, followed by the growth of these fragments synthetically, to produce lead compounds. In the present work, we planned to adopt a "reverse fragment-based drug discover approach" for the repurposing of different fragments of an already active drug (simeprevir) via the investigation of its binding to the new target, the reorientation of the fragment in this target, and/or the omission of unnecessary fragments, rather than building up a lead compound from promising fragments (standard fragment-based drug design). This approach should be distinguished from the "inverse drug discovery" approach, which identifies proteins via targeting using potent electrophiles. Thus, a set of already character-ized fragments/degradants (Figure 1) of the antiviral drug simeprevir was selected to test such an approach virtually.

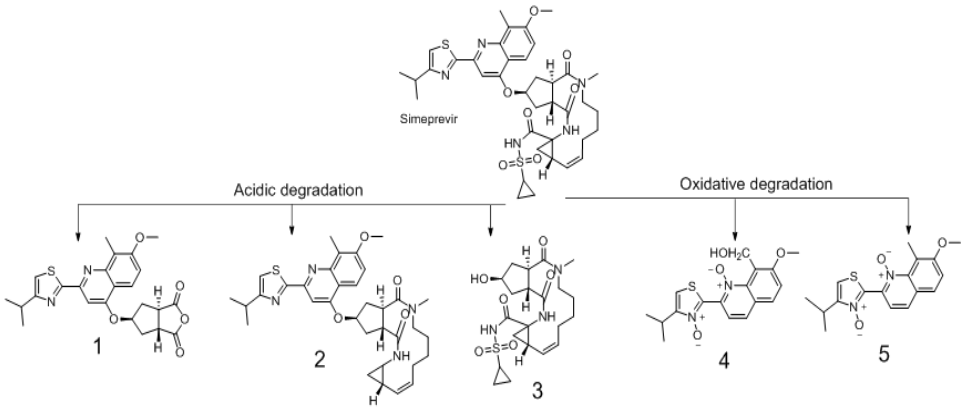

Figure 1: Simeprevir and its degradation products.

MATERIALS AND METHODS

Preparation of compounds 1–5

Compounds 1–5 were prepared and purified as reported previously[16].

In-silico ADMET study

The ADMET descriptors protocol was implemented using Discovery studio 4.0, to calculate the absorption, distribution, metabolism, excretion, and toxicity of compounds 1–5. We implemented the CHARMM force field then a small molecule protocol was used to prepare and minimize the compounds[17,18].

Docking studies

The crystal structure of the target enzyme (SARS-CoV-2 M^{pro} (PDB ID:*6* lu7, resolution: 2.16 Å)) was obtained from the Protein Data Bank (http://www.pdb.org). The docking analysis was performed using the Molecular Operating Environment (MOE)[19,43,44]. Compounds 1–5 were tested against M^{pro}, to estimate their free energies, and binding modes. At the inception, the crystal structure of M^{pro} was deprived of water, except for one essential chain, for binding. The binding pocket of the protein was defined using the co-crystallized ligand (PRD-002214) as a reference; subsequently, the protein structure was protonated, the hydrogen atoms were hidden, and the energy was minimized[20].

ChemBioDraw Ultra 14.0 was used to draw the structures of compounds **(1–5)** and the co-crystallized ligand and saved in the SDF format. Next, the MOE software was used to open the SDF files, protonate 3D structures, and minimize the energy of the molecules.

Low RMSD values were accomplished during the validation process via docking of the co-crystallized ligand solely in the target receptor[18,21]. The default protocol was followed; in each case, we generated 30 docked structures using genetic algorithm searches, followed by the visualization of the output from the MOE software, as visualized using the Discovery studio 4.0 software[17,22].

Physicochemical properties

Discovery studio 4.0 was used to determine the physicochemical properties of compounds **(1–5)**. At the start, we implemented the CHARMM force field, and then a small molecule protocol was used to prepare and minimize the compounds. The different parameters used here were calculated from the molecular properties of the small molecule protocol[20].

Cell Culture

Nawah Scientific Inc. (Mokatam, Cairo, Egypt) supplied the HSF cell line. Cells were maintained in DMEM medium supplemented with 100 mg/mL of streptomycin, 100 U/mL of penicillin, and 10% heat-inactivated fetal bovine serum in a humidified, 5% (v/v) CO_2 atmosphere at 37°C[16].

RESULTS AND DISCUSSION

Docking studies

To explore the target-binding mechanism of Simeprevir and compounds (1–5), they were docked against (Mpro) (PDB ID: 6lu7, resolution: 2.16), the major protease of SARS-CoV-2. A reference molecule was used: the co-crystallized ligand (PRD-002214). With binding free energies ranging from 6.23 to 7.65 kcal/mol, the docked compounds showed excellent binding affinities against Mpro (Table 1).

Table 1: The docking binding free energies of five compounds, simeprevir and the co-crystallized ligand (PRD-002214) against COVID-19 main protease.

Compound	Bindingfree energy (kcal/mol)
Simeprevir	-7.00
Co-crystallized ligand (PRD-002214)	-6.94
1	-6.95
2	-7.65
3	-6.23
4	-6.44
5	-6.32

The binding energy of 6.94 kcal/mol was found in the crystalline ligand (PRD-002214). The crystalline ligand had the following binding mode: Mpro's initial pocket was filled by the 2-oxopyrrolidin-3-yl molecule, which formed a hydrogen bond with Phe140. The tert-butyl carbamate moiety also filled Mpro's second pocket, making one hydrogen bond with Me49. The phenyl ring of the phenylalanine molecule also filled the third receptor pocket, producing a hydrophobic contact with His41. Finally, the fourth pocket received the ethyl propionate moiety (Figure 2, Figure 3, and Figure 4).

Simeprevir had a binding mechanism that was comparable to that of Mpro's co-crystallized ligand. It had binding energy of about 7.000 kcal/mol. Mpro's initial pocket was filled by the cyclopropane sulfonamide molecule, which formed a single hydrogen bond with Asn142.

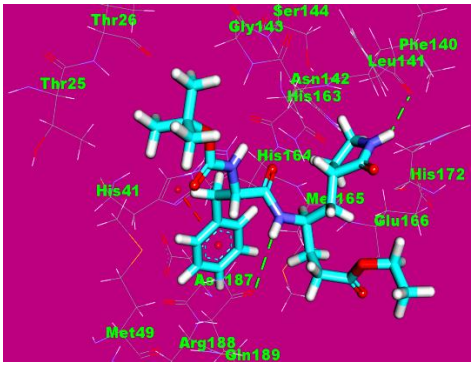

Figure 2: Co-crystallized ligand (PRD-002214) docked in to the active site of the COVID-19 main protease.

The hydrogen bonds are represented in green dashed lines, and the hydrophobic interactions are represented in orange dashed lines.

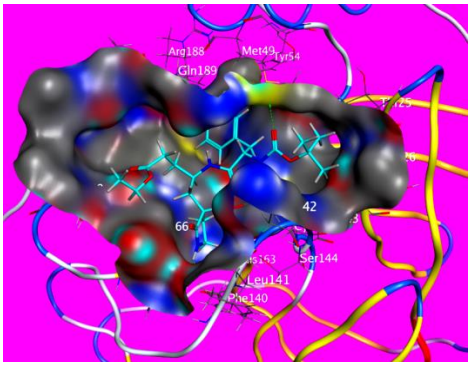

Figure 3: Mapping surface showing the co-crystallized ligand (PRD-002214) occupying the active pocket of the COVID-19 main protease.

In addition, the 5-methyl-2,3,3a,6,7,8,9,11a,12,12a,13, 14a-dodecahydrocyclo-penta [c] is a 5-methyl-2,3,3a,6,7,8,9,11a,12,12a,13, 14a-dodecahydrocyclo-penta cyclopropa[g] [1,6] The second pocket of Mpro was filled by the diazacyclo tetra decine-4,14(1H,5H)-dione moiety, which established a hydrogen connection with Met49. Furthermore, the 7-methoxy-8-methylquinoline molecule was found in the receptor's third pocket, making a hydrophobic contact with Met165. The 4-isopropylthiazole molecule was finally put into the fourth pocket, creating a hydrogen connection with Asn142 (Figure 5, Figure 6, and Figure 7). In the target-binding site, Compound **1** had a binding mechanism similar to the co-crystallized ligand and simeprevir. It occupied three Mpro pockets and had binding energy of 6.95 kcal/mol. The tetrahydro-1H-cyclopenta[c]furan-1,3(3aH)-dione moiety was found in Mpro's first pocket, where it formed two hydrogen bonds with Gly143 and Gln189. Furthermore, the 7-methoxy-8-methylquinoline moiety

filled the receptor's second pocket and formed two hydrophobic contacts with Glu166. In addition, the 4-isopropylthiazole molecule was found in the third pocket, generating two hydrophobic contacts with Pro168 (Figure 8, Figure 9, and Figure 10). In the target-binding site, Compound **2** had a binding mechanism identical to the co-crystallized ligand and simeprevir.

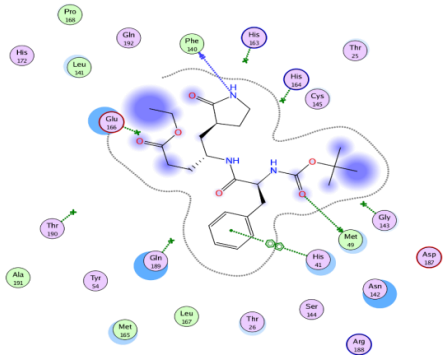

Figure 4: 2D interaction of the co-crystallized ligand (PRD-002214) in the active site of the COVID-19 main protease.

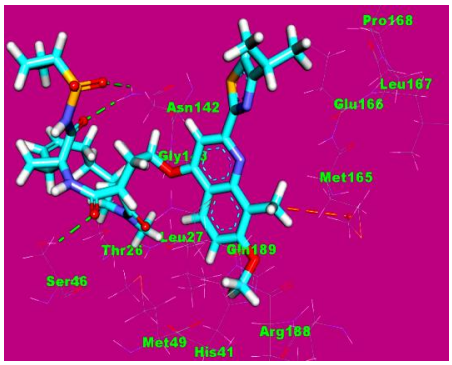

Figure 5: Simeprevir docked into the active site of the COVID-19 main protease.

Hydrogen bonds are represented in green dashed lines and the hydrophobic Interactions are represented in orange dashed lines

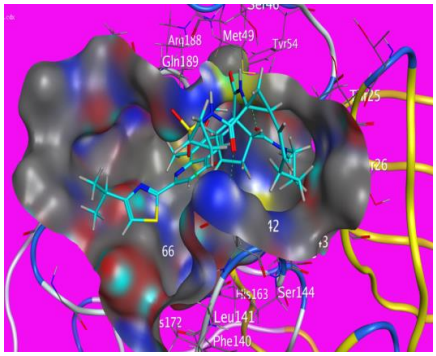

Figure 6: Mapping surface showing simeprevir occupying the active pocket of the COVID-19 main protease.

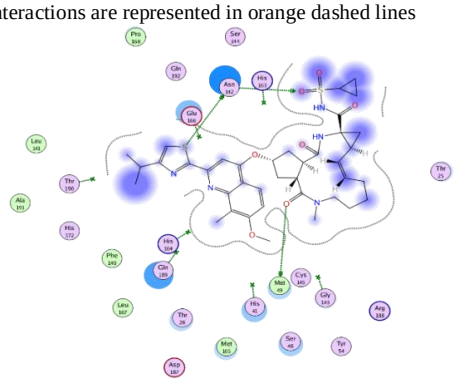

Figure 7: 2D interaction of simeprevir in the active site of the COVID-19 main protease.

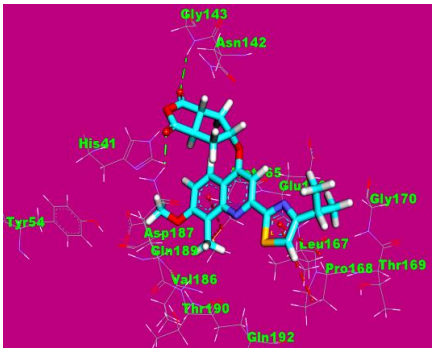

Figure 8: Compound 1 docked into the active site of COVID-19 main protease.

The hydrogen bonds are represented in green dashed lines and the hydrophobic interactions are represented in orange dashed lines.

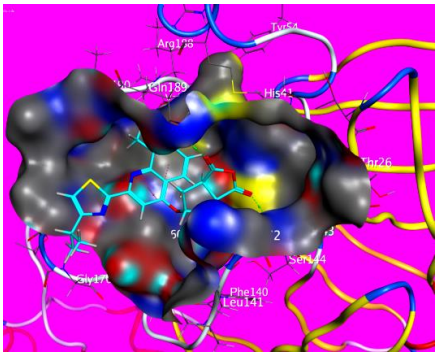

Figure 9: Mapping surface showing compound 1 occupying the active pocket of the COVID-19 main protease.

It occupied three pockets in Mpro and had the lowest binding energy (7.65 kcal/mol) of all the chemicals studied. 5-methyl- 2,3,3a,6,7,8,9,11a, 12,12a,13,14a-dodecahydro-cyclo-penta [c] is a 5-methyl-2,3,3a,6,7, 8,9,11a,12,12a, 13,14a-dodecahydrocyclo penta [c] is a 5-methyl-2 cyclopropa[g][1,6] The first pocket of Mpro was filled by the diazacyclotetra decine-4,14(1H,5H)-dione moiety, which established a hydrogen connection with Asn142. With Cys145 and His163, it also created two hydrophobic contacts. The 4-isopropylthiazole molecule was introduced into the second pocket, where it formed two hydrophobic contacts with His41 and a hydrogen bond with Thr190. Furthermore, the 7-methoxy-8-methylquinoline molecule was found in the receptor's third pocket, generating a hydrophobic contact with Pro168 (Figure 11, Figure 12, and Figure 13).

Conversely, compounds 3, 4, and 5 exhibited a lower binding affinity compared with the co-crystallized ligand (PRD-002214), with a free energy of −6.23, −6.44, and −6.32, respectively.

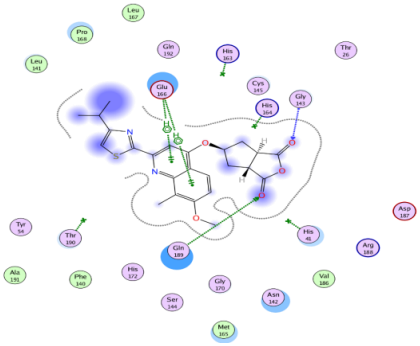

Figure 10: 2D interaction of compound 1 in the active site of the COVID-19 main protease.

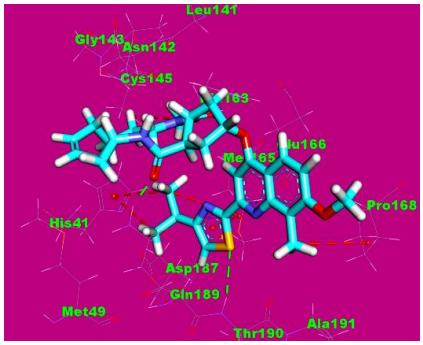

Figure 11: compound 2 docked into the active site of COVID-19 main protease.

The hydrogen bonds are represented in green dashed lines and the hydrophobic interactions in orange dashed lines and pi-anionic interaction in blue lines.

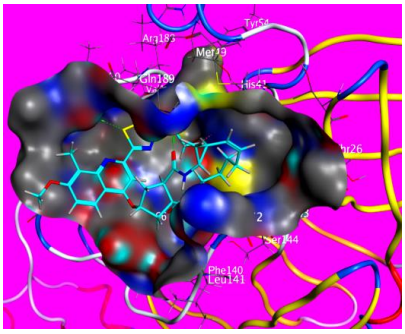

Figure 12: Mapping surface showing compound 2 occupying the active pocket of the COVID-19 main protease.

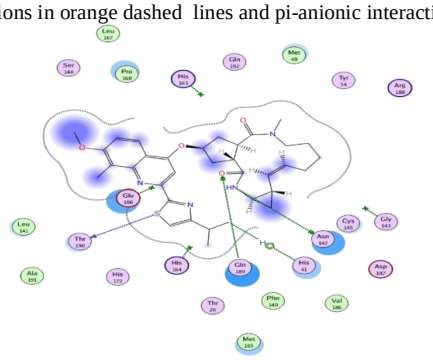

Figure 13: 2D interaction of compound 2 in the active site of the COVID-19 main protease.

In detail, compound 3 formed four hydrogen bonds with Gly143, Gln189, Asn142, and Glu166, whereas compound 4 formed two hydrogen bonds with Met49 and Glu166 and five hydrophobic interactions with Glu166, His 163, and Met165. Regarding compound 5, it formed one hydrogen bond with Glu166 and six hydrophobic interactions with His163, His41, Met165, and Glu166.

Fragment-based approach analysis

The results of the docking study (summarized in Table 2) showed that interaction with the fourth pocket of the protease was not essential for the activity of the ligand and compounds 1 and 2. Moreover, the establishment of one hydrogen bond in the first pocket was sufficient for good activity, as in the ligand, simeprevir, and compound 2. Adding one other H-bond in the first pocket yielded a lower activity, as in compound 1.

Table 2: Summarized outcomes of docking study.

Compound	Interactions with receptor	Chemical moiety (pharmacophore)
Ligand (PRD-002214) binding energy -6.95	hydrogen bond with Phe140 hydrogen bonding interaction with Met49 hydrophobic interaction with His41	the 2-oxopyrrolidin-3-yl tert-butyl carbamate the phenyl ring of phenylalanine ethyl propionate
Simeprevir binding energy -7.00	hydrogen bond with Asn142 hydrogen bond with Met49 hydrophobic interaction with Met165 hydrogen bonding interaction with Asn142	cyclopropane sulfonamide 5-methyl-2,3,3a,6,7,8,9,11a,12,12a, 13,14a-dodecahydrocyclopenta [c]cyclopropa[g][1,6]diazacyclotetra decine-4,14(1*H*,5*H*)-dione 7-methoxy-8-methylquinoline 4-isopropylthiazole
Compound 1 binding energy -6.94	two hydrogen bonds with Gly143 and Gln189 two hydrophobic interactions with Glu166 two hydrophobic interactions with Pro168	The tetrahydro-1H-cyclopenta[c]furan-1,3(3aH)-dione 7-methoxy-8-methylquinoline 4-isopropylthiazole
Compound 2 binding energy -7.65	hydrogen bond with Asn142 two hydrophobic interactions with Cys145 and His163 hydrogen bonding interaction with Thr190 two hydrophobic interactions with His41. hydrophobic interaction with Pro168	5-methyl-2,3,3a,6,7,8,9,11a,12,12a,13,14a-dodecahydrocyclopenta [c]cyclopropa[g][1,6]diazacyclotetra decine-4,14(1*H*,5*H*)-dione 4-isopropylthiazole 7-methoxy-8-methylquinoline

In contrast, adding two other hydrophobic interactions to the first pocket potentiated the activity, as in compound 2. However, the tetradecagon macrocycle was not essential; asit could be replaced with a less-complex moiety that was able to form hydrogen bonds and hydrophobic interactions. Moreover, the establishment of only one hydrophobic interaction in the third pocket yielded a better activity, similar to that achieved in the ligand, simeprevir, and compound 2 by the presence of the 7-methoxy-8-methylquinoline moiety. The presence of the 4-isopropylthiazole moiety in the second pocket afforded the essential and only hydrogen bond, as in the ligand, simeprevir, and compound 2. Furthermore, it formed two other hydrophobic interactions, which seemed to potentiate the activity, as in compound 2. In conclusion, the 7-methoxy-8-methylquinoline and 4-isopropylthiazole moieties should be retained and be located in the third and second pocket, respectively. The replacement of the tetradecagon macrocycle with a smaller moiety is recommended.

***In-silico* ADMET analysis**

Running *in-silico* ADMET studies at the early stages of compound design may reduce the risk of late-stage attrition and direct the screening procedure to choose the most promising ligands. These experiments could predict properties such as oral absorption, bioavailability, blood–brain barrier (BBB) penetration, excretion, and distribution. These properties provide important information about the dose, dose frequency, route of administration, and safety of the examined drug. Many descriptors are used in ADMET studies: I aqueous solubility, which predicts each compound's solubility in water at 25°C; ii) BBB penetration, which predicts a molecule's BBB penetration; iii) CYP2D6 binding, which predicts cytochrome P450 2D6 enzyme inhibition; iv) hepatotoxicity, which predicts if the examined compound can cause human hepatotoxicity in dose dependant manner[23].

Discovery studio 4.0 was used to predict ADMET descriptors for all compounds. The predicted descriptors are listed in Table 3. The ADMET aqueous solubility levels of compounds 3 and 4 appeared to be in the good range, whereas compound 5 showed low aqueous solubility. Conversely, compounds 1 and 2 exhibited very low solubility. ADMET BBB penetration studies predicted that the BBB penetration levels of compounds 2 and 3 were very low, whereas compound 4 exhibited low level and compounds 1 and 5 showed medium BBB penetration levels. Accordingly, all compounds were expected to be safe to the CNS.

Intestinal absorption is the percentage of a drug that is absorbed by the gut wall[24]. At least 90% of absorption into the bloodstream in humans is needed for a compound to be classified as a well-absorbed compound[25]. Moreover, poor absorption was the main reason for numerous compound failures in the clinical phase [26]. According to ADMET studies, compounds 1, 4, and 5 were expected to possess good HIA, whereas compounds 2 and 3 appeared to have moderate intestinal absorption.

Table 3: Predicted ADMET for the designed compounds and reference drugs.

Compound	BBB level[a]	Absorption level[b]	Solubility level[c]	Hepatotoxic prediction[d]	CYP2D6 prediction[e]	PPB prediction[f]
1	2	0	1	TRUE	FALSE	TRUE
2	4	1	1	TRUE	FALSE	TRUE
3	4	1	3	FALSE	FALSE	FALSE
4	3	0	3	TRUE	FALSE	TRUE
5	2	0	2	TRUE	FALSE	TRUE

[a] BBB level, blood brain barrier level, 0 = very high, 1 = high, 2 = medium, 3 = low, 4 = very low.
[b] Absorption level, 0 = good, 1 = moderate, 2 = poor, 3 = very poor.
[c] Solubility level, 1 = very low, 2 = low, 3 = good, 4 = optimal.
[d] Hepatotoxicity probability, TRUE means toxic, FALSE means non-toxic.
[e] CYP2D6, cytochrome P2D6, TRUE = inhibitor, FALSE = non inhibitor.
[f] PBB, plasma protein binding, FALSE means less than 90%, TRUE means more than 90%.

The hepatotoxicity model predicts the probable organ toxicity of a large variety of structurally varied substances[27]. Except for compound 3, all of the compounds studied were shown to exhibit some amount of hepatotoxicity. *In-vitro* and *in-vivo* research is needed to confirm these preliminary *in-silico* findings. The cytochrome P450 2D6 (CYP2D6) model, which uses the 2D chemical structure as an input, predicts CYP2D6 enzyme inhibition. The inhibition of CYP2D6 allows the impact of various medications to be amplified, potentially resulting in hazardous levels. As a result, under drug research and development regulations, a CYP2D6 inhibition trial is a requirement[28]. All examined compounds were predicted as non-inhibitors of CYP2D6. Consequently, the examined compounds are not expected to have a toxic effect from this perspective. The plasma protein binding model predicts a compound's capacity to attach to plasma proteins. This model predicts how likely a substance is to be strongly bound (90 percent binding) to blood carrier proteins[29].

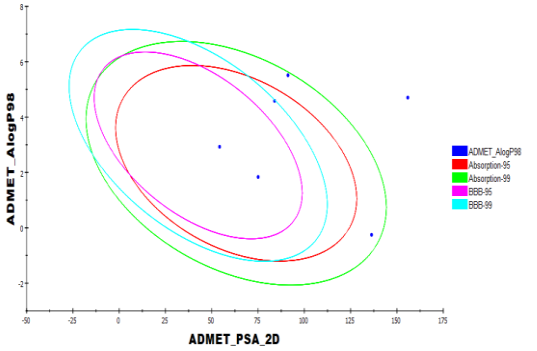

Figure 13: The expected ADMET studies.

Because the bound fraction is temporarily sheltered from metabolism, drug molecule plasma protein binding can have an impact on their efficiency. The unbound fraction, on the other hand, has therapeutic effects when it is isolated[30]. All compounds tested here were expected to exhibit >90% binding to plasma proteins, with the exception of compound 4 (Figure 13).

Physicochemical properties

The log *p* values represent the degree of lipophilicity of a chemical compound, whereas the Log D values represent the degree of lipophilicity of a chemical compound taking into account the molecule's ionization states[31]. The fact that these values have risen indicates that the lipophilic nature of the chemical under examination has improved. Compounds 1, 2, 4, and 5 have different A log *P* and LogD values, ranging from 1.928 to 5.602. These values may make it simpler for such substances to enter mucosal membranes and the lipophilic capsules of the virus.

Furthermore, the molecular polar surface area (MPSA) is a crucial parameter that affects drug bioavailability; compounds that are passively absorbed and have an MPSA of >140 have a low oral bioavailability[32]. MPSA (140) levels were found in all of the substances studied. The molecular volume (MV) descriptor also provides information on molecule transport characteristics such as GIT absorption[33]. The MV is inversely related to the drug diffusivity. Molecules with a lower MV have a higher diffusivity than those with a higher MV[34]. It is noticeable that the tested compounds exhibited low MV values compared with simeprevir (Table 4). The electric dipole moment (μ) represents the electrical effects in drug–receptor interactions[35]. The dipole moment values of the substances investigated varied from 3.2791 to 9.11863.

Table 4: Physico-chemical properties of the examined compounds.

Comp.	ALog P[a]	Log D[b]	Pka[c]	MPSA[d]	MSA[e]	MV[f]	Diploe[g]
1	4.676	4.677	3.98 4.47	115.85	437.77	354.66	3.2791
2	5.602	5.603	3.98 4.47	121.89	615.58	500.77	4.07006
3	-0.253	-0.149	2.5	141.26	428.6	358.77	7.21119
4	1.928	1.928	-	108.61	355.15	270.28	6.10701
5	3.019	3.019	-	88.38	345.41	267.88	7.40372

[a] Log of the octanol-water partition coefficient.; [b]The octanol-water partition coefficient calculated taking into account the ionization states of the molecule.; [c]The pKa of all ionizable sites.; [d] Molecular surface area: Calculates the total surface area for each molecule using a 2D approximation.
[e] Molecular polar surface area: Calculates the polar surface area for each molecule using a 2D approximation.
[f] Molecular volume: calculates the 3D volume for each molecule using the current 3D coordinates.
[g] Dipole moment: 3D electronic descriptors that indicates the strength and orientation behavior of a molecule in an electrostatic field.

Toxicity studies (*in-silico*/*in-vitro*)

Our compounds' toxicity was predicted using the Discovery studio software's proven and built models[36,37]. The ADMET research looked at the toxicity of the chemicals tested on the central nervous system and liver. The ability to assess a new drug's carcinogenic potential is dependent on its measurement[38]. As a result, three *in-silico* investigations were conducted: I the TOPKAT mouse male FDA none vs carcinogen model, which is an FDA Rodent Carcinogenicity model; and ii) the TOPKAT mouse male FDA none vs carcinogen model, which is an FDA Rodent Carcinogenicity model. The chosen model determines whether or not specific substances are carcinogenic[39].

ii) Carcinogenic potency (TD_{50}), which forecasts a chemical's median tumorigenic dose (the dosage needed to cause tumorigenesis in 50% of rats) in a prolonged exposure toxicity test[39]. The Carcinogenic Potency Data Base includes the TD_{50} measure, which has been used previously to evaluate carcinogenic potency (CPDB)[40]. iii) In a developmental toxicity potential evaluation, developmental toxicity potential indicates whether a chemical substance is likely to be hazardous. Any reversible or irreversible functional or structural alteration that interferes with and changes homeostasis, proper growth, differentiation, development, or behavior is referred to as developmental toxicity[41,42]. Three more *in-silico* studies were conducted to determine the acute and chronic toxicity of the investigated substances. I Maximum tolerated dose (MTD) for rats, which forecasts the greatest dose of a drug that will provide the intended effect without generating undesirable side effects[43,44], ii) rat oral LD_{50}, which forecasts a chemical's rat oral acute median fatal dosage (LD_{50}) in toxicity tests[45]. iii) The rat chronic least observed adverse effect level (LOAEL), which forecasts a chemical's rat chronic LOAEL[45].

In-silico, most chemicals demonstrated relatively little unfavourable effects and toxicity against the evaluated models, as shown in Table 5. With the exception of compound 3, all compounds seemed to be non-carcinogenic in the FDA Rodent Carcinogenicity Model. Compounds 1 and 2 had low TD50 values in the carcinogenic potency TD50 mouse model, but compounds 2, 4, and 5 had high TD50 values. The tested compounds showed MTDs ranging from 0.006 to 0.020 g/kg of body weight in the rat MTD model. Furthermore, in the developmental toxicity potential model, all chemicals were non-toxic. All drugs had modest oral LD50 values in the rat oral LD50 paradigm, ranging from 0.080 to 0.352 mg/kg of body weight/day. Finally, the compounds' LOAELs in the rat chronic LOAEL model varied from 0.005 to 0.023 g/kg of body weight. The toxicity of a chemical structure is very crucial for the validation of its use as a drug. Thus, it was of interest to check the toxicity of the tested structures. The SRB assay was used to assess the potential toxicity and/or safety of simeprevir and its

degradation products (1–5) against a human skin fibroblast (HSF) normal cell line at five different concentrations (0.01, 0.1, 1, 10, and 100 µM) in comparison with a standard drug (doxorubicin, positive control). The SRB assay showed a lack of observed alterations of cell viability, with the exception of compound 3, for which a slight cytotoxicity was noticed, in accordance with the *in-silico* study. These results were also confirmed by the recording of morphological changes via optical microscopy images. Simeprevir and compounds 1–5 were demonstrated to be non-toxic up to 100 µM (IC_{50}> 100 µM)[16].

Table 5: Toxicity properties of compounds.

Compound	1	2	3	4	5
TOPKAT_mouse_male_ FDA_none_vs_carcinogen model	Non-carcinogen	Non-carcinogen	Carcinogen	Non-carcinogen	Non-carcinogen
Carcinogenic Potency TD_{50} Mouse [a]	11.613	3.910	33.345	47.454	73.882
Developmental Toxicity Potential	Toxic	Non-Toxic	Non-Toxic	Non-Toxic	Non-Toxic
Rat Maximum Tolerated Dose [b]	0.018	0.006	0.012	0.020	0.013
Rat Oral LD_{50} [b]	0.300	0.352	0.290	0.115	0.080
Rat Chronic LOAEL[b]	0.011	0.005	0.005	0.019	0.023

[a]Unit: mg/kg body weight/day; [b]Unit: g/kg body weight.

CONCLUSIONS

The molecular docking study of the antiviral simeprevir and its degradants 1–5 proved that simeprevir and its degradants 1 and 2 could be added to the protocol of treatment of SARS-COV-2. A docking study revealed the higher binding affinity of simeprevir and compound 2 compared with the natural ligand, whereas compound 1 showed equal affinity to the natural ligand. In contrast, compounds 3–5exhibited a lower binding affinity. ADMET and toxicity studies confirmed that compounds 1 and 2 are safe to the CNS, non-toxic, non-carcinogenic, and expected to be orally bioavailable. The approach highlighted in this study could be defined as "reverse FBDD," in which different fragments of an already active candidate (simeprevir) were inspected, its binding was identified, and reorientation of particular fragments in the active site was performed, to afford the best binding. The removal of unnecessary fragments (e.g., cyclopropane sulfonamide) from already active drug/compounds is recommended, rather than building up compounds from active fragments using the standard "FBDD" approach.

ACKNOWLEDGEMENTS

The authors would like to acknowledge the Faculty of Pharmacy, University of Sadat City for the facilities offered to run this study in their labs.

AUTHORS' CONTRIBUTIONS

El-Behairy MF: conceptualization, methodology, correspondence. **Fayed MAA**: conceptualization, writing original draft preparation. **Ahmed RM**: data curation, writing-original draft preparation. **Abdallah IA:** methodology, writing-review and editing.

DATA AVAILABILITY

Data will be made available on reasonable request.

CONFLICT OF INTEREST

None to declare.

REFERENCES

1. Di Gennaro F, Pizzol D, Marotta C, *et al*. Coronavirus Diseases (COVID-19) current status and future perspectives: A Narrative Review. Int J Env Res Public Health 2020;17 (8): 2690. *https://doi.org/10.3390/ijerph17082690*
2. Scannell JW, Blanckley A, Boldon H, Warrington B. Diagnosing the decline in pharmaceutical R&D efficiency. Nature Reviews Drug Discov 2012; 11(3):191-200. *https://doi.org/10.1038/nrd3681*
3. Drews J. Drug discovery: A historical perspective. Sci 2000; 287(5460):1960-1964. *https://doi.org/10.1126/science.287.5460.1960*
4. Phatak SS, Stephan CC, Cavasotto CN. High-throughput and *in silico* screenings in drug discovery. Expert Opin Drug Discov 2009;4 (9): 947-959. *https://doi.org/10.1007/978-981-10-3573-9_11*
5. Congreve M, Murray CW, Blundell TL. Keynote review: Structural biology and drug discovery. Drug Discovery Today 2005; 10(13):895-907. *https://doi.org/10.1016/S1359-6446(05)03484-7*
6. Cavasotto CN, Aucar MG, Adler NS. Computational chemistry in drug lead discovery and design. Int J Quantum Chem 2019; 119(2): e25678. *https://doi.org/10.1002/qua.25678*
7. Serafin MB, Bottega A, Foletto VS, da Rosa TF, Hörner, A, Hörner R. Drug repositioning is an alternative for the treatment of coronavirus COVID-19. Int J Antimicro Agents 2020; 105969. *https://doi.org/10.1016/j.ijantimicag.2020.105969*
8. Dhir N, Jain A, Mahendru D, Prakash A, Medhi B. Drug Repurposing and Orphan Disease Therapeutics 2020. *https://doi.org/10.5772/intechopen.91941*
9. Talevi A, Bellera CL. Challenges and opportunities with drug repurposing: Finding strategies to find alternative uses of therapeutics. Expert Opin Drug Discov 2019;15(4): 397-401. *https://doi.org/10.1080/17460441.2020.1704729*
10. Sohraby F, Bagheri M, Aryapour H. Performing an *in silico* repurposing of existing drugs by combining virtual screening and molecular dynamics simulation. Methods Molecular Biol (Clifton, N.J.) 2019; 1903: 23-43. *https://doi.org/10.1007/978-1-4939-8955-3_2*
11. Senanayake SL. Drug repurposing strategies for COVID-19. Future Drug Discov 2020;2(2). *https://doi.org/10.4155/fdd-2020-0010*
12. You DM, Pockros PJ. Simeprevir for the treatment of chronic Hepatitis C. Expert Opin Pharmacoth 2013;14(18): 2581-9. *https://doi.org/10.1517/14656566.2013.850074*
13. Shereen MA, Khan S, Kazmi A, Bashir N, Siddique R. COVID-19 infection: Origin, transmission, and characteristics of human coronaviruses. J Adv Res 2020;24: 91-98. *https://doi.org/10.1016/j.jare.2020.03.005*

14. Dai W, Zhang B, Su H, *et al*. Structure-based design of antiviral drug candidates targeting the SARS-CoV-2 main protease. Science 2020; eabb4489. *https://doi.org/10.1126/science.abb4489*
15. Flanagan S, Crawford-Jones A, Orkin C. Simeprevir for the treatment of hepatitis C and HIV/hepatitis C co-infection. Exp Rev Clin Pharmacol 2014;7(6):691-704. *https://doi.org/10.1586/17512433.2014.956091*
16. Ahmed RM, Fayed MAA, El-Behairy MF, Abdallah IA. Identification, isolation, structural characterization, *in silico* toxicity prediction and *in vitro* cytotoxicity assay of simeprevir acidic and oxidative degradation products. RSC Advances 2020; 10(70): 42816-42826. *https://doi.org/10.1039/d0ra09253c*
17. El-Zahabi MA, Elbendary ER, Bamanie FH, *et al*. Design, synthesis, molecular modeling and anti-hyperglycemic evaluation of phthalimide-sulfonylurea hybrids as PPARγ and SUR agonists. Bioorg Chem 2019; 91: 103115. *https://doi.org/10.1016/j.bioorg.2019.103115*
18. Ibrahim MK, Eissa IH, Alesawy MS, *et al*. Design, synthesis, molecular modeling and anti-hyperglycemic evaluation of quinazolin-4 (3H)-one derivatives as potential PPARγ and SUR agonists. Bioorg Med Chem 2017;25(17): 4723-4744. *https://doi.org/10.1016/j.bmc.2017.07.015*
19. Chemical Computing Group, Molecular Operating Environment (MOE).
20. El-Gamal KM, El-Morsy AM, Saad AM, *et al*. Synthesis, docking, QSAR, ADMET and antimicrobial evaluation of new quinoline-3-carbonitrile derivatives as potential DNA-gyrase inhibitors. J Mol Struct 2018;1166: 15-33. *https://doi.org/10.1016/j.molstruc.2018.04.010*
21. Elmetwally SA, Saied KF, Eissa IH, Elkaeed EB. Design, synthesis and anticancer evaluation of thieno [2, 3-d] pyrimidine derivatives as dual EGFR/HER2 inhibitors and apoptosis inducers. Bioorg Chem 2019;88:102944. *https://doi.org/10.1016/j.bioorg.2019.102944*
22. Mahdy HA, Ibrahim MK, Metwaly AM, *et al*. Design, synthesis, molecular modeling, *in vivo* studies and anticancer evaluation of quinazolin-4 (3H)-one derivatives as potential VEGFR-2 inhibitors and apoptosis inducers. Bioorg Chem 2020; 94: 103422. *https://doi.org/10.1016/j.bioorg.2019.103422*
23. Van De Waterbeemd H, Gifford E. ADMET *in silico* modelling: Towards prediction paradise? Nature Revi Drug Discov 2003;2(3): 192-204. *https://doi.org/10.1038/nrd1032*
24. Mannhold R, Kubinyi H, Folkers G. Pharmacokinetics and metabolism in drug design. John Wiley & Sons: 2012; 51.
25. Klopman G, Stefan LR, Saiakhov RD. ADME evaluation: 2. A computer model for the prediction of intestinal absorption in humans. European J Pharm Sci 2002;17(4-5): 253-263. *https://doi.org/10.1016/s0928-0987(02)00219-1*
26. Patel H, Dhangar K, Sonawane Y, *et al*. In search of selective 11β-HSD type 1 inhibitors without nephrotoxicity: An approach to resolve the metabolic syndrome by virtual based screening. Arabian J Chem 2015. *https://doi.org/10.1016/j.arabjc.2015.08.003*
27. Hewitt M, Przybylak K. *In silico* models for hepatotoxicity. In *in silico* methods for predicting drug toxicity. Springer 2016; 201-236.
28. Roy PP, Roy K. QSAR studies of CYP2D6 inhibitor aryloxypropanolamines using 2D and 3D descriptors. Chem Biol Drug Design 2009;73(4): 442-455. *https://doi.org/10.1111/j.1747-0285.2009.00791.x*
29. Ghafourian T, Amin Z. QSAR models for the prediction of plasma protein binding. BioImpacts: BI 2013;3(1):21. *https://doi.org/10.5681/bi.2013.011*
30. Smith DA, Di L, Kerns EH. The effect of plasma protein binding on *in vivo* efficacy: Misconceptions in drug discovery. Nature Reviews Drug Discov 2010; 9(12):929-939. *https://doi.org/10.1038/nrd3287*
31. Eissa IH, El-Naggar AM, El-Sattar NE, Youssef AS. Design and discovery of novel quinoxaline derivatives as dual DNA intercalators and topoisomerase II inhibitors. Anti-Cancer Agents Med Chem 2018; 18(2):195-209. *https://doi.org/10.2174/1871520617666170710182405*
32. Utilizing MA, HFF. American Chemical Society. J Am Chem Soc 1977;99(25): 8127-8134.
33. Liang Y, Xu QS, Li HD, Cao DS. Support vector machines and their application in chemistry and biotechnology. CRC Press: 2016.
34. Ansel HC, Popovich NG, Allen LV. Pharmaceutical dosage forms and drug delivery systems. Williams & Wilkins Baltimore: 1995; 6.
35. Lien EJ, Guo ZR, Li RL, Su CT. Use of dipole moment as a parameter in drug receptor interaction and quantitative structure activity relationship studies. J Pharm Sci 198;71 (6):641-655. *https://doi.org/10.1002/jps.2600710611*
36. Xia X, Maliski EG, Gallant P, Rogers D. Classification of kinase inhibitors using a Bayesian model. J Med Chem 2004; 47(18):4463-4470. *https://doi.org/10.1021/jm0303195*
37. BIOVIA QSAR, ADMET and Predictive Toxicology.
38. Heidelberger C. Chemical carcinogenesis. Annual Rev Biochem 1975; 44 (1): 79-121. *https://doi.org/10.1146/annurev.bi.44.070175.000455*
39. Venkatapathy R, Wang NCY, Martin TM, Harten PF, Young D. Structure–Activity Relationships for Carcinogenic Potential. General Applied Syst Toxicol 2009. *https://doi.org/10.1002/9780470744307.gat079*
40. Thresher A, Gosling JP, Williams R. Generation of TD 50 values for carcinogenicity study data. Toxicol Res 2019;8 (5):696-703. *https://doi.org/10.1039/c9tx00118b*
41. Louisse J, Bosgra S, Blaauboer BJ, Rietjens IM, Verwei, M. Prediction of *in vivo* developmental toxicity of all-trans-retinoic acid based on *in vitro* toxicity data and *in silico* physiologically based kinetic modeling. Arch Toxicol 2015; 89(7):1135-1148. *https://doi.org/10.1007/s00204-014-1289-4*
42. EPA Guidelines for Developmental Toxicity Risk Assessment.
43. Goodrnan G, Wilson R. Comparison of the dependence of the TD50 on maximum tolerated dose for mutagens and nonmutagens. Risk Analys 1992;12(4):525-533.
44. Council NR. Correlation between carcinogenic potency and the maximum tolerated dose: implications for risk assessment. In Issues in Risk Assessment, National Academies Press (US): 1993.
45. Diaza RG, Manganelli S, Esposito A, *et al*. Comparison of *in silico* tools for evaluating rat oral acute toxicity. SAR QSAR Env Res 2015;26(1):1-27. *https://doi.org/10.1080/1062936X.2014.977819*
46. Venkatapathy R, Moudgal CJ, Bruce RM. Assessment of the oral rat chronic lowest observed adverse effect level model in TOPKAT, a QSAR software package for toxicity prediction. J Chem Inform Comp Sci 2004;44(5):1623-1629. *https://doi.org/10.1021/ci049903s*